Magnetic field effect on the chiral magnetism of noncentrosymmetric UPtGe: Experiment and theory

Atsushi Miyake,[1,*] Leonid M. Sandratskii,[2,†] Ai Nakamura,[3] Fuminori Honda,[3] Yusei Shimizu,[3] Dexin Li,[3] Yoshiya Homma,[3] Masashi Tokunaga,[1] and Dai Aoki[3]

[1]*Institute for Solid State Physics, The University of Tokyo, Kashiwa, Chiba 277-8581, Japan*
[2]*Max-Planck-Institute for Microstructure Physics, Weinberg 2, Halle, D-06120, Germany*
[3]*Institute for Materials Research, Tohoku University, Oarai, Ibaraki, 311-1313, Japan*

(Received 20 August 2018; revised manuscript received 2 November 2018; published 28 November 2018)

The effect of differently oriented magnetic field on chiral incommensurate helimagnet UPtGe is studied both experimentally and theoretically. The magnetization measurements up to the field above the saturation have revealed an isotropic magnetic response below 20 T and a remarkable nonmonotonic anisotropy in high fields. Moreover, the two principally different phase transitions from the noncollinear incommensurate to the field-induced ferromagnetic state have been observed. These properties are successfully explained by density-functional theory calculations taking into account the noncollinearity of the magnetic structures, arbitrary directed magnetic field, and relativistic effects. We also estimate the strength of different competing magnetic interactions and discuss possible scenarios of the field-induced phase transformations.

DOI: 10.1103/PhysRevB.98.174436

I. INTRODUCTION

Uranium intermetallic compounds show a wide variety of electronic properties, owing to the delicate balance of the hybridization between U $5f$ electrons and conduction electrons of ligand elements and competing interaction energy scales [1]. One of the intriguing phenomena observed in uranium based compounds is the coexistence of ferromagnetism (FM) and superconductivity [2–4]. Applying magnetic fields reveals new unexpected phenomena of these materials: e.g., the reentrance of the superconductivity is induced in URhGe when the magnetic field of 12 T is applied along the hard magnetization axis initiating spin-reorientation transition [5]. Obviously, the strength of the magnetic anisotropy (MA) plays an important role in the formation of such intriguing physical phenomena. In contrast to the Ising-like ferromagnet URhGe, UPtGe is a unique U system showing a chiral incommensurate helical magnetic ordering below $T_N \sim 51$ K [6]. In the model of the helix suggested in Ref. [7] the MA was considered to be negligibly small. The spin dynamics was recently studied via the NMR experiments, and the XY-type spin fluctuations were clarified [8]. The chiral helical structures in various types of materials have been attracting strong research interest because of their importance in the physics of skyrmion lattices and chiral domains, topics of intense study in the field of spintronics [9–11].

A number of neutron diffraction studies lead to the same conclusion that the magnetic ground state of UPtGe is an incommensurate cycloid propagating along the a axis with the wave vector $\vec{q} = [0.55 - 0.57, 0, 0]$ in units of $2\pi/a$; the U moments lie in the ac plane [6,12–14]. Importantly, Mannix *et al.* [6] clarified that the orthorhombic crystal structure of UPtGe is of the noncentrosymmetric EuAuGe type ($Imm2$, space group No. 44) (Fig. 1), which is different from the centrosymmetric TiNiSi type, such as of URhGe, or $CeCu_2$ type assumed in previous studies [12–16]. Another important property revealed in the experiment is a chiral character of the cycloid [6]: All domains have the same wave vector $\vec{q}$ whereas the domains with opposite wave vector $-\vec{q}$ are absent.

Previously proposed explanation [7] of the origin of the incommensurate cycloid in UPtGe includes the following components: (i) a very small MA in the cycloid plane, which was treated as negligible, (ii) competing interatomic exchange interactions, and (iii) an active Dzyaloshinskii-Moriya interaction (DMI) due to the lack of the inversion symmetry. The first two features explain the formation of the incommensurate cycloid, and the third is responsible for the chiral character of the magnetic ground state. An important conclusion of Ref. [7] is a critical sensitivity of the magnetic structure to the crystal lattice [17].

The study of the response of UPtGe to the magnetic field is expected to deepen the understanding of chiral incommensurate magnetism and of the field induced incommensurate-commensurate (I-C) phase transitions, which are fascinating phenomena of solid state physics. Despite the long history of the studies on this topic (see, e.g, early reviews [18,19]) the understanding of the I-C transitions is by far not complete. There are some exact statements, which are based on very simple theoretical models, like sine Gordon equation [20,21]. The applicability of these models to complex real materials is not self-evident. There are also more complex theoretical models solved numerically, e.g., atomistic spin Hamiltonians [22]. However, such models are sensitive to the values of a large number of parameters whose choice is not unique.

We report a joint experimental and theoretical study of the magnetic field effect on UPtGe. The magnetization measurements are performed in fields up to 56 T that are above

*Corresponding author: miyake@issp.u-tokyo.ac.jp
†Corresponding author: lsandr@mpi-halle.mpg.de

 ©2018 American Physical Society

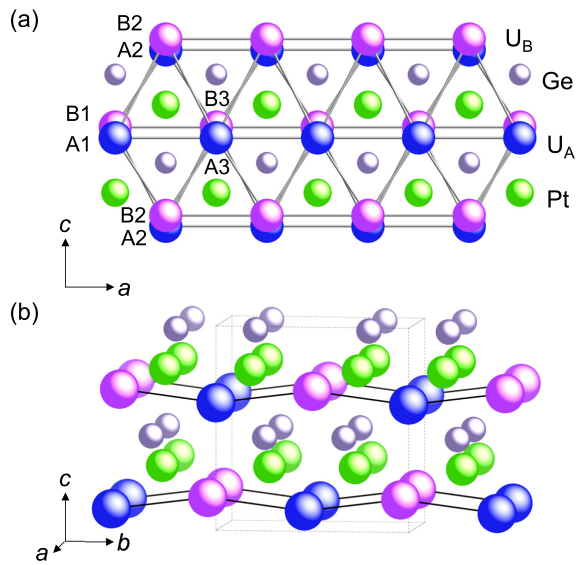

FIG. 1. Crystal structure of UPtGe projected on the (a) *ac* and (b) *bc* planes. There are two inequivalent U sublattices referring U_A and U_B, whose closest neighbors are Pt and Ge atoms, respectively [15]. The U atoms lying in the same *ac* plane form a distorted hexagonal lattice formed by the atoms of both sublattices. The labels of U atoms in (a) are used in Table I. Along the *b* axis the U atoms of two sublattices form zigzag chains.

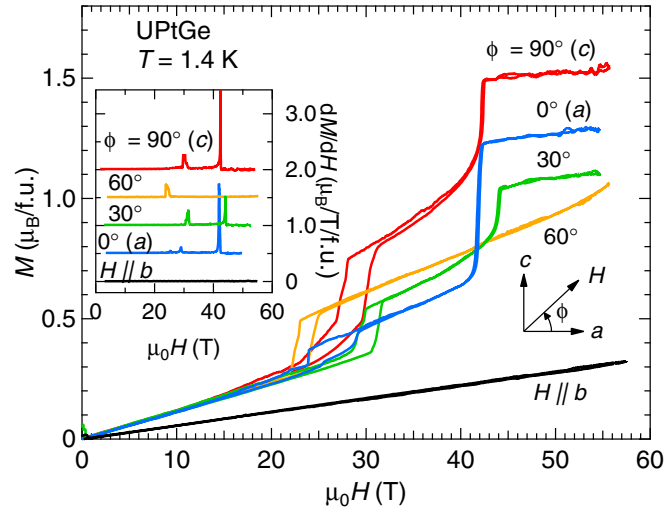

FIG. 2. Magnetization $M(H)$ curves of UPtGe at $T = 1.4$ K for various field directions. The inset shows the differential susceptibility $\mathrm{d}M/\mathrm{d}H$ for each increasing-field sweep. $\mathrm{d}M/\mathrm{d}H$ are offset by 0.5 μ_B/T/f.u. for the sake of clarity.

the saturation field for field directions in the cycloid plane. The isotropic behavior observed in low fields is replaced at higher fields by anisotropic field-induced phase transitions. This raises new important questions that we address on the basis of the density-functional theory (DFT) calculations. One of the focuses of our attention is the complex interplay of various interactions responsible for the unusual physical properties of UPtGe. Other focus is the field-induced phase transitions. Our experiment reveals the sequence of two very different phase transformations bringing the system from the chiral incommensurate helical state to the field-induced ferromagnetic state [23].

II. EXPERIMENT

Single crystals of UPtGe were prepared using the Czochralski pulling method in a tetra-arc furnace. Pulsed magnetic fields were generated using nondestructive magnets installed at the International MegaGauss Science Laboratory of the Institute for Solid State Physics at the University of Tokyo. The conventional induction method using coaxial pick-up coils was used for the magnetization measurements down to 1.4 K.

III. RESULTS OF EXPERIMENT

Magnetization $M(H)$ curves for various field directions are presented in Fig. 2. The anisotropy between the *ac* plane and out-of plane *b* axis is very large. For $H \parallel b$, the magnetization is H linear without any anomalies and much smaller than for the field in the *ac* plane. In the following, we focus on the field directions in the cycloidal *ac* plane. Angle ϕ defining field direction is measured from the orthorhombic *a* axis. Below 20 T, the magnetization is nearly isotropic. This isotropic magnetic response seems to be expected in connection with the assumed negligibly small in-plane MA [7]. By contrast, two remarkable anisotropic increments of magnetization are seen at about 25 T and 42 T (Fig. 2) revealing the presence of considerable MA in the *ac* plane. The observed high-field anisotropy is nonmonotonic with respect to the field direction. Indeed, the saturated magnetic moment is maximal for the field parallel to the *c* axis ($\phi = 90^\circ$). It strongly drops for $\phi = 60^\circ$ and then increases again for $\phi = 30^\circ$ and $\phi = 0^\circ$ (*a* axis) (Fig. 2). For $\phi = 60^\circ$, magnetization shows upturn near the maximum fields but does not saturate up to the maximum fields.

IV. METHOD OF CALCULATION

To understand the unusual angular dependence of the in-plane MA, we performed the calculation of the energy of the FM configuration for different directions of the atomic moments with respect to the crystallographic axes. The calculations were carried out with the augmented spherical waves code [24,25] able to deal with noncollinear magnetism, spin-orbit coupling, and magnetic field along an arbitrary direction [26,27]. Since the localization of the $5f$ states can be underestimated in standard DFT calculations, we performed additional calculations introducing a scaling parameter $\alpha < 1$ to study the sensitivity of the results to the level of the $5f$-states localization. This parameter is used as a scaling factor for interatomic Hamiltonian and overlap integrals of U $5f$ wave functions entering the secular matrix. The exchange-correlation potential was used in the local density approximation (LDA) [28]. The **k**-vector sampling suggested by Monkhorst and Pack [29] was employed in the integration over the Brillouin zone (BZ). The description of the crystal structure of the EuAuGe type and lattice parameters of UPtGe determined in the neutron diffraction experiment can be found in Ref. [6]. In the calculations for orthorhombic unit cell

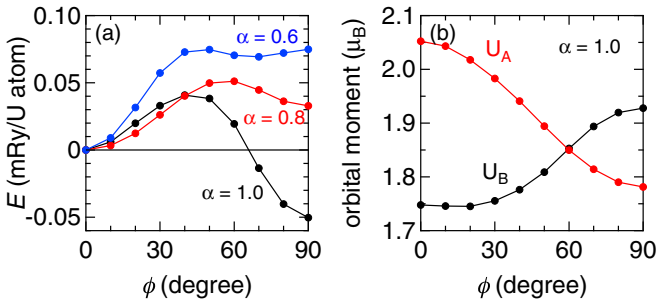

FIG. 3. (a) Magnetic anisotropy energy for the FM configurations and (b) orbital moments of the two U sublattices as a function of ϕ.

containing four U atoms the number of the **k** points in the BZ varied between 8000 and 27 000. For larger unit cells the number of the **k** points decreased in accordance with decreasing BZ volume. In very long-lasting calculations of self-consistent magnetic structures in large supercells the reduced numbers of the k points were used.

V. RESULTS OF CALCULATIONS AND DISCUSSION

A prominent feature of the theoretical ϕ dependence of the magnetic anisotropy energy, $E(\phi)$ [Fig. 3(a)] is its nonmonotonic character, which is consistent with the $M(H,\phi)$ curves (Fig. 2). An insight into the origin of the nonmonotonic $E(\phi)$ is provided by the consideration of the ϕ dependence of the orbital moments of the two inequivalent U sublattices [see Fig. 3(b)], since there is deep physical connection between MA energy and orbital moments anisotropy (see, e.g., Refs. [30,31]). The calculations gave the remarkable result that the orbital moments of the two U sublattices, though both monotonic functions of ϕ, have opposite character: decrease for the A sublattice and increase for the B sublattice. The competition of two opposite angular dependences explains unexpected properties of the MA of UPtGe: its unusual smallness for U compounds and the nonmonotonic behavior. The calculations with reduced overlap of the $5f$ functions scaled with parameter $\alpha = 0.8$ show that the nonmonotonic behavior of the $E(\phi)$ is a robust property [Fig. 3(a)]. For the stronger scaling with parameter $\alpha = 0.6$, the nonmonotonic features become weak.

After we have revealed the presence of sizable in-plane MA for the FM structures, we would like to reveal the origin of the isotropic response below 20 T (Fig. 2). A direct DFT calculation of the response of an incommensurate magnetic structure to differently oriented magnetic field is not feasible because of an infinite magnetic unit cell of the incommensurate structure. Therefore, we performed the following calculations to address this problem. We selected two parts of the helix with different directions of the atomic moments with respect to the crystal lattice [see Fig. 4(a)] and described these pieces with the supercells corresponding to commensurate helix with $q = 0.5$. In the first supercell, the initial directions of the atomic moments are collinear to the a and c axes [Fig. 4(b)]. In the second, the moments were rotated by 45° [Fig. 4(c)]. Next we calculate the magnetic response to the field of 23.5 T [32] applied along different directions. We obtained two opposite monotonic dependencies of the induced

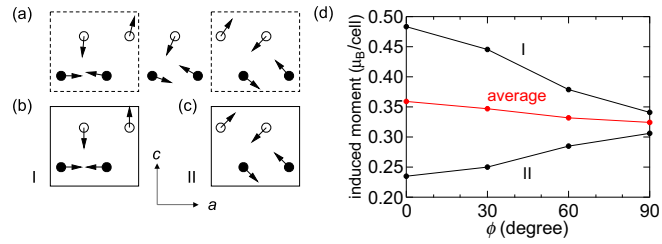

FIG. 4. (a) Schematic picture of an incommensurate cycloid with wave vector $q = 0.527$. The open (full) symbols correspond to U_A (U_B), respectively. (b) Supercell I corresponding to $q = 0.5$ and atomic moments parallel to the a and c axes. (c) Supercell II: atomic moments rotated by 45° with respect to supercell I. (d) The induced magnetic moments of supercells I, II, and their average as a function of ϕ. The supercells presented in (b) and (c) have an increased size of $2a$ along the a axis. Only the atoms laying in the same ac plane are shown.

moment on the field direction ϕ for two supercells [Fig. 4(d)]. This property explains the isotropy of the response of the cycloid to the applied magnetic field below 20 T as the result of the averaging of the anisotropic responses of different parts of the cycloid.

It is worth noting that the contributions of the orbital and spin moments to the induced moment shown in Fig. 4(d) have opposite signs: positive for the orbital moment and negative for the spin moment. The ratio of the magnitudes of the induced orbital and spin moments varies for the points of the 'average' line in the interval between 2.2 and 2.4. The fact that the induced spin moment is opposite to the direction of the magnetic field reveals stronger influence of the third Hund's rule than the direct influence of the Zeeman coupling to the field (see also Ref. [27]).

It is important to compare the energy scales of different magnetic interactions, i.e., interatomic exchange interaction, DMI, and Zeeman energy. First, we estimate the interatomic exchange parameters. As a reference state of the system, we used the FM configuration with atomic moments parallel to the a axis. To estimate the exchange interaction parameter between atoms i and j in Fig. 1(a), we evaluated the energies of the magnetic configurations with the moments of atoms i and j deviated in the ac plane by angle 10° in the same and opposite directions (see Fig. 5). The difference of these

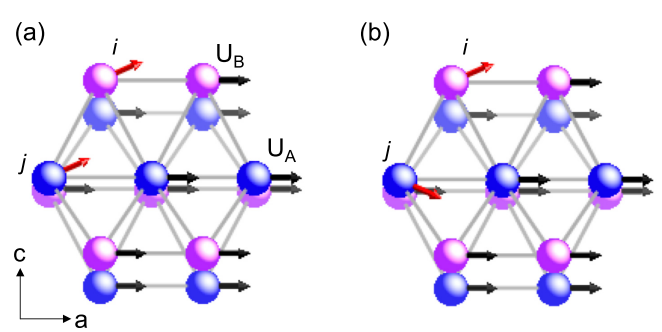

FIG. 5. The difference of the energies of the two magnetic configurations (a) and (b) gives an estimation of the exchange interaction parameter J_{ij} between atoms i and j.

TABLE I. Interatomic exchange parameters J_{ij} in the units of mRy.

i, j	$\alpha = 1.0$	$\alpha = 0.8$	$\alpha = 0.6$
A1, B1	0.275	0.821	1.373
A1, A2	−0.013	−0.014	−0.014
A1, B2	−0.076	0.009	0.139
A1, A3	−0.202	−0.239	0.061
A1, B3	−0.047	−0.105	−0.123
B1, B2	−0.058	−0.017	−0.0257
B1, B3	−0.014	0.061	0.082

energies estimates the exchange energy corresponding to the angle 20° between moments of the atoms i and j. By dividing the energy by $[1 - \cos(20^\circ)]$, we obtain exchange parameter J_{ij}. The values of the calculated exchange parameters are listed in Table I.

For unscaled calculation ($\alpha = 1.0$), only exchange parameter $J_{\mathrm{A1,B1}}$ is FM. It corresponds to the interaction between neighboring atoms of the zigzag chain (Fig. 1). This interaction is the strongest among all estimated interatomic exchange interactions. This result supports the picture of ferromagnetically ordered zigzag chains [6,13,14]. The decrease of the overlap given by $\alpha < 1$, on one hand, increases the values of atomic moments and, on the other hand, diminishes the quantum-mechanical interaction integrals. Therefore, there is no *a priori* way to relate the change in the electronic overlap to the character of the variation of interatomic exchange interaction. Indeed, the analysis of exchange parameters presented in Table I shows that there is no general trend in the variation of the exchange interactions with decreasing scaling parameter. For the calculation without scaling, all exchange parameters with the exception of the interchain one are antiferromagnetic (AFM) that leads to the frustration and canting of the atomic moments. The strongest AFM interaction is $J_{\mathrm{A1,A3}}$ [Fig. 1(a)], while $J_{\mathrm{B1,B3}}$ is remarkably weak. For scaling factor $\alpha = 0.8$ the values of parameters are in good correlation with those for unscaled calculations. For stronger scaling with $\alpha = 0.6$ the exchange interactions become distinctly more FM.

The chiral magnetism of UPtGe essentially arises from the DMI [7]. The strength of DMI is calculated as the difference of the energies of the cycloids with $q = 0.5$ and $q = -0.5$ and has the following values: 0.11 mRy/U for unscaled calculation, 0.21 mRy/U for $\alpha = 0.8$, and 0.22 mRy/U for $\alpha = 0.6$. This estimation shows that the energy scale of the DMI is of the same order of magnitude as the exchange interaction. We also obtained considerable dependence of the DMI strength on the localization parameter.

Finally, we estimate the scale of the Zeeman energy. The orientation of atomic moments parallel to the magnetic field gives the energy gain of $\mu_0 H M$ where M is the value of the atomic magnetic moment per U atom. At 40 T and $M = 1.25\,\mu_{\mathrm{B}}$ we obtain the value of $\mu_0 H M \sim 0.21$ mRy/U, which is close to the values of the AFM exchange interactions (see Table I).

As shown above the calculations give a complex balance of several interactions. The chiral magnetic ground state of UPtGe comes from competing exchange interactions and contributions of the DMI and MA. In applied magnetic fields, the Zeeman energy overcomes these interactions, leading to the FM transformation.

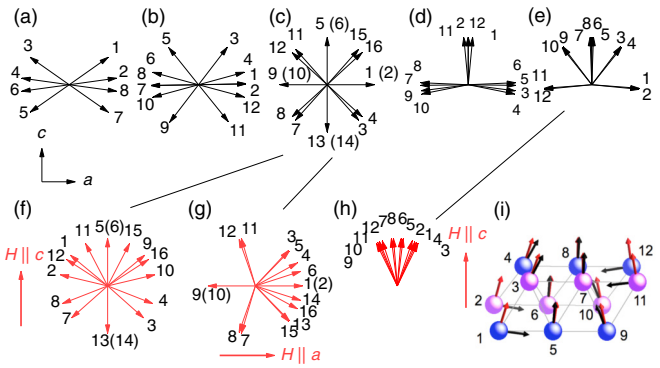

FIG. 6. Examples of self-consistent magnetic structures. (a)–(e) Magnetic structures without applied magnetic field. Magnetic structures (f) for $H \parallel c$ and (g) for $H \parallel a$ based on the magnetic structure (c). (h) Magnetic structure for $H \parallel c$ based on the magnetic structure (e). (i) Space resolved presentation of structures (e) and (h) with correspondingly black and red vectors. The numbering of atoms is shown in (i). The number of the U atom in the supercell is 8 for structure (a), 12 for structures (b), (d), (e), and (h), and 16 for structures (c), (f), and (g). The supercells were obtained by extending the unit cell along the a axis.

Now we turn to the discussion of the two field-induced phase transitions (Fig. 2). The applicability of the direct DFT calculations to the description of these phase transitions is rather limited [33]. Nevertheless, it is instructive to perform the following calculations. We consider supercells of different moderate sizes and start the iterational process with various accidentally chosen magnetic configurations. The magnetic moments are allowed to relax to a self-consistent state. On the next step, we apply the magnetic field and consider the change of the magnetic configurations. The calculations with self-consistently determined directions of the magnetic moments were performed as follows. In the first step, the calculations were carried out with a relatively small number of k points in the BZ that varied from about 200 for the supercell containing eight U atoms to about 50 for the supercell with 16 U atoms. When the convergence of the directions of all U moments reached 0.1° the number of k points was approximately doubled and the calculations continued until the convergence of the directions is better than 0.01° [34].

The analysis of performed calculations shows that starting from different initial magnetic configurations we generally obtain different self-consistent magnetic states. Among the self-consistent states there are both magnetically compensated [see examples in Figs. 6(a)–6(c)] and uncompensated states [Figs. 6(d) and 6(e)]. The fact that the calculations give multiple self-consistent states indicates the presence of numerous local minima in the complex high-dimensional energy landscape describing the energy of the system as a function of the directions of atomic moments.

Figures 6(f), 6(g) and 6(h) show the result of the calculations with external field of 100 T. In Figs. 6(f) and 6(g), we present the transformation of the compensated magnetic structure (c) in the fields directed along the c and a axes, respectively. For both field directions there is the modification

of the magnetic structure resulting in an induced magnetic moment. The response to the magnetic field is anisotropic. The induced net spin, orbital, and total magnetic moments along field direction for structure (f) are, respectively, −3.68, 7.60, and 3.92 μ_B per supercell. For structure (g) these values are larger: −6.92, 12.37, and 5.45 μ_B. The energies of the in-field structures (f) and (g) are lower than the energy of the compensated structure (c) by 6.2 and 3.1 mRy, respectively. The decreases in the Zeeman energy are, however, only 2.0 and 2.7 mRy per supercell. This reveals that self-consistent response of the electron system to the applied field is considerably more complex than a rotation of the rigid atomic moments.

Figure 6(h) shows the transformation of the uncompensated magnetic structure (e) with the field along the c axis. Interestingly, in this case the modification of the magnetic structure is especially strong and the in-field state is rather close to the FM state. The numerical results give the following values: the differences of the net spin, orbital, and total moments of the structures (h) and (e) are −9.3, 16.3, and 7.0 μ_B per supercell. The energy of structure (h) is lower than that of structure (e) by 5.9 mRy, whereas the difference of the Zeeman energies of the two structures is only 3.5 mRy per supercell.

We remark that the magnetic field used in the calculations presented in Figs. 6(f), 6(g) and 6(h) is about two times larger than the maximal experimental field. This large field was selected to make the influence of the field clearly visible in the figures. The property that this field does not lead in all cases to the magnetic structure close to ferromagnet is explained as follows. The energy of the system as a function of the directions of the atomic moments is a very complex unknown function with many local minima and barriers separating these minima. It is to be expected that these barriers are often higher than the characteristic Zeeman energies even for large magnetic fields. In the DFT calculations we deal with electron interactions that are of larger scale. Since in the calculations there are no fluctuations that can be responsible for the tunneling of the system from a local minimum to a deeper minimum the system remains near one of the quasistable states. It is also important that we can perform calculations only for relatively small supercells whereas in the I-C transitions the intermediate structures with larger period can be important. This makes the problem of the quantitative theoretical description of the system very challenging. Our paper makes a step towards this description but remains on the level revealing qualitatively new properties.

Coming back to our experiment, we remark that the interpretation of the lower-field phase transition at around 25–30 T is rather straightforward. The system transforms discontinuously in a magnetically uncompensated fan-type structure. The examples of such a structure are shown in Figs. 6(d) and 6(e) [35].

The nature of the higher-field phase transition to the ferromagnetic state around 40 T is principally different, as clearly seen in Fig. 2. First, it does not have a noticeable hysteresis. Second, the $M(H)$ curves just below the transition have a strong convex curvature. There are two possible scenarios of this transition. One possibility is a special property of the energy landscape of UPtGe consisting in (i) almost equal energies of the fan structure just before the transition and the ferromagnetic structure after the transition and (ii) the existence of a barrier-free path between these points of the energy landscape. The process resembling this type of transformation is obtained in our numerical experiments [Figs. 6(e), 6(h) and 6(i)]. This calculation shows that the system can, in principle, relatively easily move from the fan configuration to the state close to collinear ferromagnetism.

As an alternative scenario, we mention the possibility of soliton-lattice formation. Here, with increasing fields the regions of noncollinear magnetic moments are separated by increasing ferromagnetically aligned domains (see, e.g., figures in Refs. [21,36] illustrating this kind of transition). The convex $M(H)$ curve and hysteresis-free transitions are characteristic features of the soliton-lattice type transition [21] which is consistent with the in-field behavior obtained as the solution of the sine-Gordon equation.

It is possible that both scenarios contribute to the transition. The neutron diffraction or resonant x-ray scattering studies of the transitions would be very useful but are challenging in such high-field regions. On the theoretical side, one can study the energetics of the system using a lattice spin model. However, a very large crystal domain must be used to describe the structures of different periodicity, and a large number of parameters must be employed to reflect the complexity of the system. Though further progress appears rather laborious, we hope that our work will stimulate new deep studies on the I-C transition of the chiral helical magnetic structures.

VI. SUMMARY

We have reported the magnetic properties of chiral incommensurate magnet UPtGe in the fields of varying directions and up to above the saturation. We have revealed that magnetic response, isotropic for fields below 20 T, becomes strongly anisotropic for higher fields where two principally different phase transitions are observed. Remarkably, this anisotropy possesses an unusual nonmonotonic field-orientation dependence. Our DFT calculations successfully explain the apparently contradicting properties obtained in the low- and high-field experiments with the identification of competing contributions into magnetic interactions, magnetic anisotropy, and magnetization process. We suggest an interpretation of the nature of the two phase transitions that bring the system from the incommensurate to the field-induced ferromagnetic state. Our work deepens the understanding of the physical origin of the wide variety of the properties of the U intermetallics.

ACKNOWLEDGMENTS

The authors are grateful to A. Pourret and Y. Tokunaga for fruitful discussions. This research was carried out (in part) at the International Research Center for Nuclear Materials Science, Institute for Materials Research, Tohoku University. This work was partially supported by the MEXT of Japan Grants-in-Aid for Scientific Research (JP15K17700, JP15K05156, JP15H05882, JP15K05884, JP15K21732, JP15KK0149, and JP16H04006).

[1] V. Sechovsky and L. Havela, in *Handbook of Magnetic Materials*, edited by K. H. Bushow (Elsevier, Amsterdam, 1998), p. 1.

[2] D. Aoki, A. Huxley, E. Ressouche, D. Braithwaite, J. Flouquet, J.-P. Brison, E. Lhotel, and C. Paulsen, Nature (London) **413**, 613 (2001).

[3] N. T. Huy, A. Gasparini, D. E. de Nijs, Y. Huang, J. C. P. Klaasse, T. Gortenmulder, A. de Visser, A. Hamann, T. Görlach, and H. V. Löhneysen, Phys. Rev. Lett. **99**, 067006 (2007).

[4] D. Aoki and J. Flouquet, J. Phys. Soc. Jpn. **81**, 011003 (2013).

[5] F. Lévy, I. Sheikin, B. Grenier, and A. D. Huxley, Science **309**, 1343 (2005).

[6] D. Mannix, S. Coad, G. H. Lander, J. Rebizant, P. J. Brown, J. A. Paixão, S. Langridge, S. Kawamata, and Y. Yamaguchi, Phys. Rev. B **62**, 3801 (2000).

[7] L. M. Sandratskii and G. H. Lander, Phys. Rev. B **63**, 134436 (2001).

[8] Y. Tokunaga, A. Nakamura, D. Aoki, Y. Shimizu, Y. Homma, F. Honda, H. Sakai, T. Hattori, and S. Kambe, Phys. Rev. B **98**, 014425 (2018).

[9] S. Mühlbauer, B. Binz, F. Jonietz, C. Pfleiderer, A. Rosch, A. Neubauer, R. Georgii, and P. Boni, Science **323**, 915 (2009).

[10] S. Heinze, K. V. Bergmann, M. Menzel, J. Brede, A. Kubetzka, R. Wiesendanger, G. Bihlmayer, and S. Blügel, Nat. Phys. **7**, 713 (2011).

[11] K. v. Bergmann, A. Kubetzka, O. Pietzsch, and R. Wiesendanger, J. Phys.: Cond. Matter. **26**, 394002 (2014).

[12] A. Szytula, M. Kolenda, R. Troc, V. H. Tran, M. Bonnet, and J. Rossat-Mignod, Solid State Commun. **81**, 481 (1992).

[13] S. Kawamata, K. Ishimoto, Y. Yamaguchi, and T. Komatsubara, J. Magn. Magn. Mater. **104**, 51 (1992).

[14] R. A. Robinson, A. C. Lawson, J. W. Lynn, and K. H. J. Buschow, Phys. Rev. B **47**, 6138 (1993).

[15] R.-D. Hoffmann, R. Pöttgen, G. H. Lander, and J. Rebizan, Solid State Sci. **3**, 697 (2001).

[16] All three crystal structures have similar positions of the U atoms but differ in the positions of the Pt and Ge atoms, resulting in the breaking of the inversion symmetry and two inequivalent types of U atoms in the case of EuAuGe structure.

[17] The calculations performed for the TiNiSi lattice gave a FM ground state in drastic disagreement with experiment. This is the first point of the sensitivity of the calculational results to the details of the employed theoretical model. Another point is the sensitivity to the localization of the $5f$ states discussed below.

[18] P. Bak, Rept. Progr. Phys. **45**, 587 (1982).

[19] Y. A. Izyumov, Sov. Phys. Usp. **27**, 845 (1984).

[20] I. E. Dzyaloshinskii, Sov. Phys. JETP **20**, 665 (1965).

[21] Y. Togawa, Y. Kousaka, K. Inoue, and J. Kishine, J. Phys. Soc. Jpn. **85**, 112001 (2016).

[22] J. Jensen, Phys. Rev. B **54**, 4021 (1996).

[23] There are two possible references to the metamagnetic phase with saturated magnetization: field-induced ferromagnet or field-polarized paramagnet. Since in this paper we focus on the low-temperature region well below T_N, where the fluctuations characteristic for the paramagnetism of the localized moments are absent, we prefer to use the notion of field-induced ferromagnet.

[24] A. R. Williams, J. Kübler, and C. D. Gelatt, Phys. Rev. B **19**, 6094 (1979).

[25] V. Eyert, *The Augmented Spherical Wave Method*, Lecture Notes in Physics, Vol. 849 (Springer-Verlag, Berlin, Heidelberg, 2012).

[26] L. M. Sandratskii, Adv. Phys. **47**, 91 (1998).

[27] L. M. Sandratskii, Phys. Rev. B **94**, 184414 (2016).

[28] U. von Barth and L. Hedin, J. Phys. C **5**, 1629 (1972).

[29] H. J. Monkhorst and J. D. Pack, Phys. Rev. B **13**, 5188 (1976).

[30] P. Bruno, Phys. Rev. B **39**, 865 (1989).

[31] L. M. Sandratskii, Phys. Rev. B **92**, 134414 (2015).

[32] This field corresponds to the spin splitting of electron levels by 0.1 mRy.

[33] One of the limitations is the necessity to use large supercells. Another limitation is the absence in the standard DFT calculations of the fluctuations responsible in the nature for the realization of the first order phase transitions.

[34] This type of the calculations is very time consuming since the relaxation of the magnetic moments is a complex and slow process. The attempt to speed up this process by increasing the step of the movement of the moments at each iteration usually leads to the disconvergence of the calculation. Therefore, we had to limit the number of this type of calculations and to use relatively small super cells. The total number of such calculations was about 25. Representative examples of the results of these calculations are presented in Fig. 6.

[35] The fan structure stabilized by the magnetic field is expected to be commensurate although its period in the case of UPtGe is not known.

[36] A. Zheludev, S. Maslov, G. Shirane, Y. Sasago, N. Koide, and K. Uchinokura, Phys. Rev. B **57**, 2968 (1998).